Computational and Structural Biotechnology Journal 23 (2024) 990–1004

Contents lists available at ScienceDirect

Computational and Structural Biotechnology Journal

journal homepage: www.elsevier.com/locate/csbj

Research article

Comprehensive integration of single-cell RNA and transcriptome RNA sequencing to establish a pyroptosis-related signature for improving prognostic prediction of gastric cancer

Jie Li [1], Tian Yu [1], Juan Sun, Mingwei Ma, Zicheng Zheng, Weiming Kang [*], Xin Ye [*]

Department of General Surgery, Peking Union Medical College Hospital, Chinese Academy of Medical Sciences & Peking Union Medical College, No.1 Shuaifu Yuan, Dongcheng District, 100730 Beijing, People's Republic of China

ARTICLE INFO

Keywords:
Cell pyroptosis
Gastric cancer
Single-cell RNA sequencing
Immune infiltration
Prognostic signature

ABSTRACT

Cell pyroptosis, a Gasdermin-dependent programmed cell death characterized by inflammasome, plays a complex and dynamic role in Gastric cancer (GC), a serious threat to human health. Therefore, the value of pyroptosis-related genes (PRGs) as prognostic biomarkers and therapeutic indicators for patients needs to be exploited in GC. This study integrates single-cell RNA sequencing (scRNA-seq) dataset GSE183904 with GC transcriptome data from the TCGA database, focusing on the expression and distribution of PRGs in GC at the single-cell level. The prognostic signature of PRGs was established by using Cox and LASSO analyses. The differences in long-term prognosis, immune infiltration, mutation profile, CD274 and response to chemotherapeutic drugs between the two groups were analyzed and evaluated. A tissue array was used to verify the expression of six PRGs, CD274, CD163 and FoxP3. C12orf75, VCAN, RGS2, MKNK2, SOCS3 and TNFAIP2 were successfully screened out to establish a signature to potently predict the survival time of GC patients. A webserver (https://pumc.shinyapps.io/GastricCancer/) for prognostic prediction in GC patients was developed based on this signature. High-risk score patients typically had worse prognoses, resistance to classical chemotherapy, and a more immunosuppressive tumor microenvironment. VCAN, TNFAIP2 and SOCS3 were greatly elevated in the GC while RGS2 and MKNK2 were decreased in the tumor samples. Further, VCAN was positively related to the infiltrations of Tregs and M2 TAMs in GC TME and the CD274 in tumor cells. In summary, a potent pyroptosis-related signature was established to accurately forecast the survival time and treatment responsiveness of GC patients.

1. Introduction

Gastric cancer (GC) is one of the common malignant tumors worldwide, with high morbidity and mortality [1]. China is one of the high-incidence areas of GC, accounting for about 40% of the global annual new cases and deaths [2]. Although the comprehensive treatment of GC is constantly updated and improved, its 5-year overall survival rate remains dismal [3]. In recent years, immunotherapy was the first-line therapy for advanced cancer, but only a few patients with GC can benefit from the treatment of immune checkpoint inhibitors (ICIs) [4,5]. It has been reported that multi-gene signatures can effectively elevate the survival time and treatment response to chemotherapy or immunotherapy of GC patients [6,7]. Hence, it is urgent to investigate and establish appropriate biomarkers to forecast the prognosis and treatment response of patients for selecting the optimal therapies to prolong the survival time of patients with GC.

Cell pyroptosis is an identified way of regulated cell death, which is characterized by the continuous expansion until the cell membrane ruptures, resulting in releasing cell contents and triggering strong inflammatory responses [8–10]. Further, cell pyroptosis not only exerts its critical roles in immune response, antagonizing infections and transmitting endogenous signals and but is also involved in the initiation and progression of tumors [11–14].

Single-cell RNA sequencing (scRNA-seq) eliminates heterogeneity in

Abbreviations: GC, gastric cancer; scRNA-seq, single-cell RNA sequencing; PRGs, pyroptosis-related genes; DEGs, differentially expressed genes; PCA, principal component analysis; OS, overall survival; ICIs, immune checkpoint inhibitors; TME, tumor microenvironment; IHC, immunohistochemistry; TAMs, tumor-associated macrophages; Tregs, regulatory T cells.

* Correspondence authors.
E-mail addresses: Kangwm@pumch.cn (W. Kang), yexinpumch@163.com (X. Ye).

[1] #These authors contributed equally to this study.

https://doi.org/10.1016/j.csbj.2024.02.002
Received 9 October 2023; Received in revised form 4 February 2024; Accepted 4 February 2024
Available online 7 February 2024

tissues by clustering cells, which is of significance for the progress of precision therapy [15]. In addition, scRNA-seq can accurately evaluate the role of genes in specific cell types, which is more conducive to the exploration of molecular mechanisms in initiation and development of malignancies [16,17]. In view of the abovementioned advantages, more and more studies have identified novel biomarkers by integrating scRNA-seq and bulk RNA-seq. Hence, we decided to integrate scRNA-seq and transcriptome RNA-seq to establish a signature for improving prognostic prediction and optimizing the selection of therapeutic methods of GC by using bioinformatics analysis.

In this research, we constructed a pyroptosis-related signature to potently forecast the survival time and treatment response of GC by integrating scRNA-seq and transcriptome RNA-seq. The survival difference was clearly discriminated between the two groups divided by the pyroptosis-related signature. Patients with high risk scores not only had shorter survival times but also were more resistant to classical chemotherapy drugs and prone to immunosuppressive tumor microenvironment (TME) in GC. Additionally, *MKNK2*, *RGS2*, *TNFAIP2*, *VCAN*, *SOCS3*, *C12orf75*, *CD274*, *CD163* and *FoxP3* were detected in the tissue array of GC. In summary, a potent signature was constructed to accurately forecast the survival time and treatment responsiveness of GC patients using six pyroptosis-related genes (PRGs).

2. Materials and methods

2.1. Tissue specimen

The tissue array containing 54 paired GC tissues and corresponding adjacent tissues was gathered from the Department of General Surgery, Peking Union Medical College Hospital (PUMCH) from September 2021 to December 2022. The pathological results of GC in patients were validated by physicians from the Department of Pathology of PUMCH. Dissected tissues were fully soaked and fixed in liquid formaldehyde and embedded in paraffin within one week for subsequent long-term preservation and immunohistochemical staining. All patients signed a consent form with full knowledge before the tissue samples were collected. This study was permitted by the Ethical Committee of PUMCH (I-22PJ035).

2.2. Data collection

In this study, we selected 24 primary gastric cancer tumor samples from the GSE183904 dataset [18]. The TCGA data used in this analysis, including the TPM profile, Count data matrix, somatic mutation data, survival data and clinical information of each patient, were from UCSC Xena. We used the annotation file provided by UCSC Xena to re-annotate the data with Gene Symbol before subsequent analysis. Then, we sorted out the clinical data containing age, gender, pathological stage and survival time. To meet the standards of analysis, we only retained GC patients with complete prognostic information to establish a prognostic signature. Finally, the GSE62254 containing 300 samples and the intact clinical information was utilized to verify the accuracy of the pyroptosis-related signature in the prognostic prediction of GC patients [19].

2.3. Quality control of scRNA-seq data using Seurat

The platform for detecting scRNA-seq data was Illumina NovaSeq 6000. The result matrix of Seurat (version 4.0) R package imported the GSE183904 creates the Seurat object for this analysis [20]. The selection criteria were stringent. Firstly, we included samples that exhibited gene/feature expression shared by three or more cells in each sample. Secondly, only cells displaying gene expression of 500 or more features but fewer than 6000 features were considered. Additionally, we excluded cells with a mitochondrial RNA percentage greater than 20%. “DoubletFinder” was employed to identify doublets using the gene-expression data [21]. These rigorous selection criteria and quality control steps were implemented to ensure the high quality and reliability of our data. The data were first quality-controlled by the original standard, and 118887 cells were selected for further analysis. Next, the GSE183904 dataset is standardized by the ’NormalizeData’ function. The subsequent data processing was consistent with the published literature [6]. Then, according to the ElbowPlot function with variable genes as input, principal component analysis (PCA) is utilized to identify significant principal components (PCs). The top 30 PCs are selected as the statistically significant input of t-Distributed Stochastic Neighbor Embedding (t-SNE) (dims = 30).

2.4. Cluster analysis and cell type annotation of scRNA-seq

Cell clustering and cell type identification of cell clusters were analyzed by ’FindClusters’ function. In addition to annotating cell types, ScType software also identified the annotations of cell type and further searched for differential marker genes between cell populations [22]. The ’FindAllMarkers’ function compares the expression of genes between different cell types using the Wilcoxon rank sum test to identify differential genes between cell types.

2.5. Differential expression of PRGs in cells

51 PRGs are gathered from the Molecular Signatures Database and published literature [23]. Supplementary Table S1 provided detailed information on 51 PRGs. The overlapping results of PRGs and differentially expressed genes (DEGs) between cell types were identified by the Venn diagram software package. The heatmap showed the expression of these overlapping results in different immune cells by using the ’DoHeatmap’ function. Their expression in GC and adjacent tissues were compared in the TCGA dataset and statistically significant by t-test. When the p-value < 0.05, it was significant.

We utilized the AUCell package’s AUCell_calcAUC function to compute the PRG activity levels for each cell and analyzed the average PRG activity within various cell types. Subsequently, we categorized these cells into high pyroptosis and low pyroptosis groups based on the median value of PRG activity. The DEGs between the two groups of cells were further analyzed by the ’FindAllMarkers’ function, which used the Wilcoxon rank sum test. Then, genes specifically expressed in the high-pyroptosis group were selected as DEGs related to pyroptosis in GC for subsequent analysis.

2.6. KEGG and GO enrichment analysis

The R package clusterProfiler (version 4.2.0) was utilized to conduct KEGG pathway enrichment on DEGs related to pyroptosis to identify significantly enriched biological processes [24]. Gene Ontology (GO) enrichment was also used to analyze the DEGs related to pyroptosis from large-scale functional enrichment at different dimensions and levels. Fisher’s exact test was used to calculate the significance of each term. The significant threshold of enrichment analysis was p value < 0.05, and the enrichment results are further visualized by bubble plots.

2.7. Construction of a prognostic signature

A prognostic signature was constructed using the TPM profile of GC samples with complete survival data in the TCGA dataset. Univariate Cox analysis was used to preliminarily identify PRGs associated with the overall survival (OS) of GC patients. Subsequently, LASSO analysis was used to screen out the prominent genes, and multivariate Cox analysis was further used to construct a prognostic signature. The risk score calculation formula is:

$$riskScore = \sum_{i}^{n} Coef(gene_i) * Expression(gene_i)$$

Coef ($gene_i$), expression ($gene_i$) and n represent the coefficient of multivariate Cox regression, the expression of each gene and the number of genes, respectively.

2.8. Construction of a predictive nomogram

The risk scores and clinicopathological features were incorporated through the RMS package (version: 5.1–4) to generate a nomogram and calibration curve. The calibration curve is evaluated by mapping the predicted survival probability to the actual survival probability, and the 45° line represents the best predictive value. Subsequently, the survival package was used to draw a forest map to visualize the effects of each clinicopathological features (gender, age, T stage, N stage, M stage and AJCC stage) and risk score on prognosis.

2.9. An online prediction tool for survival probability of GC patients

A webserver containing a dynamic nomogram was built up to forecast the survival probability of GC patients using the "DynNom" and "Shiny" R packages based on the Shiny website (https://www.shinyapps.io/). Detailed user guides, including how to use the server, interpret the output results, and apply the results to specific issues, were provided in the supplementary File S1.

2.10. Estimation of immune cell infiltration

CIBERSORTx is an analytical tool for evaluating immune cell infiltration [25]. The assumed immune cell abundance was estimated using a reference set containing 22 immune cell subtypes and 1000 permutations. Combined with the LM22 characteristic gene matrix, the samples with p value < 0.05 were screened out to obtain the immune cell infiltration matrix. Then the data with immune cell enrichment fraction greater than zero are retained, and the final results of immune cell infiltration matrix are obtained. Pearson correlation analysis was performed on the infiltrating immune cells and 6 PRGs.

2.11. Immune infiltration and immune checkpoint analysis based on the pyroptosis-related signature

The abundance of immune cells in two groups was compared. The correlation between risk scores and immune cell infiltration was analyzed by Spearman correlation. In addition, common immune checkpoints (ICG_genes_pmid_310434170) were compared in two groups. The relationship between CD274 and PRGs in the signature was analyzed. P value < 0.05 was considered significant.

2.12. Analysis of somatic mutations and chemosensitivity

The somatic mutation data of TCGA-STAD were acquired through the R package of 'TCGAbiolinks', sorted into the mutation annotation format file, and analyzed using the R package 'maftools'. The method of chemosensitivity analysis was consistent with previous publication [6].

2.13. Immunohistochemistry (IHC)

The procedures of IHC were consistent with the previous publications [26,27]. First, tissue sections were deparaffinized in xylene and rehydrated through graded alcohol. Second, antigen repair was performed according to the corresponding requirements. Third, endogenous peroxidase was blocked by 3% hydrogen peroxide. Fourth, 3% bovine serum albumin was used to block the tissue sections. Fifth, *VCAN* (Sangon Biotech, D223532), *TNFAIP2* (Sangon Biotech, D123384), *RGS2* (Sangon Biotech, D221197), *MKNK2* (Sangon Biotech, D225598), *SOCS3* (Abcam, ab280884), *C12orf75* (Signalway antibody, #37781), *CD274* (Abcam, ab282458), *CD163* (Abcam, ab182422), and *FoxP3* (Abcam, ab215206) are the primary antibodies used in the IHC staining. The dilution ratio of each primary antibody was under the product instructions. Two fields of each tissue were randomly chosen under the 40 × objective lens. Then, Image-Pro Plus software was used to evaluate the expression of each protein using the integrated optical density (IOD) method consisting of staining area and intensity. The sum of the IOD of two random fields is the final IOD value of each tissue.

2.14. Statistics analysis

R (version 4.1) (https://www.r-project.org/) was used to conduct the data calculations and statistical analyses. Analysis of transcriptome RNA sequencing and scRNA-seq data were statistically significant at p value < 0.05 or adj. p value < 0.05.

3. Results

3.1. Identification of cell type by scRNA-seq analysis

As shown in Fig. 1, the flow chart presented the detailed procedures of this study. First, the scRNA-seq data of 118887 cells from 24 GC patients was obtained from GSE183904 dataset after strictly screening with quality control. Fig. S1A presented the detected gene numbers, the depth of sequencing and the gene ratio of mitochondrial and hemoglobin in each specimen. 3000 variable genes were chosen to further analysis after data normalization (Fig. S1B). PCA analysis was used to reduce dimensionality and visualize the data, and the top 30 PCs were selected as the input of t-SNE (Fig. S1C). The results of t-SNE shown that the total cells were divided into 33 clusters (Fig. S1D and Fig. 2A). 33 clusters were classified into 11 cell types (cancer cells, $CD8^+$ NKT−like cells, endothelial, mast cells, memory B cells, memory $CD8^+$ T cells, myeloid cells, neuroendocrine cells, neutrophils, non−classical monocytes and stromal cells) by using ScType (Fig. 2B). In addition, the specific number of each cell type was presented in Fig. 2C. Moreover, the proportion of cell type was also investigated in each GC sample (Fig. 2D). The violin plot revealed the most representative marker gene in each cell type (Fig. 2E). Furthermore, the top 10 marker genes in each cell type were also demonstrated (Fig. 2F). In summary, 11 cell types were successfully classified by using the scRNA-seq data of 118887 cells.

3.2. Screening of differentially expressed PRGs in GC

To investigate the role of pyroptosis in GC, 51 PRGs were extracted from the Molecular Signatures Database and published literature [23]. The results of Venn diagram produced the 9 overlapping differentially expressed PRGs between the PRGs and marker genes (Fig. 3A). The expression of 9 PRGs (*CHMP2A*, *CHMP4B*, *CYCS*, *GZMB*, *HMGB1*, *IL1B*, *IRF1*, *GPX4* and *PYCARD*) was investigated in GC at single cell level and presented with violin plots (Fig. S2) and t-SNE distribution (Fig. S3), from which we can find that most of PRGs were enriched in immune-related cells. In addition, the heatmap shown the expression of 9 differentially expressed PRGs in each cell type (Fig. 3B). Notably, CHMP4B and CHMP2A are significantly upregulated in cancer cells; GZMB and IRF1 show increased expression in T cells; IL1B, PYCARD, and GPX4 are significantly upregulated in Myeloid cells. Additionally, GPX4 also shows increased expression in Mast cells and Neuroendocrine cells. HMGB1 is upregulated in Endothelial cells; IL1B is increased in Non-classical monocytes, and CYCS is upregulated in Neuroendocrine cells. These analyses will help to better understand the mechanisms of action of PRGs in gastric cancer and their specific roles in different cell types (Fig. S2 and Table S2). The results of GO analysis indicated that the 9 PRGs mainly exerted its role on the regulation of immune cells (Fig. 3C and Table 1). Furthermore, the PRGs not only acted the role of pyroptosis, but also affected the process of cell apoptosis and necroptosis by the KEGG analysis (Fig. 3D and Table 1), which was in consistent with previous studies [28].

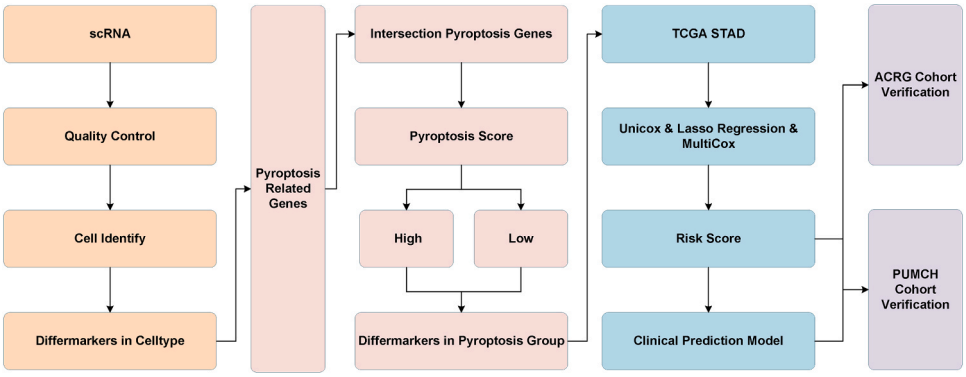

Fig. 1. The analysis flow of this study.

3.3. Scoring the cell type based on the expression of 9 PRGs

Due to the critical roles of pyroptosis in tumor progression, we scored each cell on the basis of 9 PRGs expression by using the 'AUCell' function. The t-SNE distribution displayed the pyroptosis score of each cell (Fig. 4A). We compared the PRG activity among different cell types, with Myeloid cells and monocytes exhibiting higher PRG activity, while CD8 + NKT-like cells displayed the lowest activity (Fig. 4B). Then, we divided the cells into two groups (high-pyroptosis and low-pyroptosis) according to the median value of pyroptosis score. The t-SNE offered a visual distribution of two groups at single cell level, from which we can learn that high-pyroptosis of cell mainly enriched in the cancer cells, myeloid cells and non−classical monocytes (Fig. 4C). Volcanic plot presented the DEGs between the GC and adjacent normal tissues through analyzing the transcriptome RNA sequencing from TCGA (Fig. 4D). The 1209 DEGs in high-pyroptosis group were screened through comparing with the low-pyroptosis group. Next, 152 overlapping DEGs were obtained after comparing the DEGs and 1209 DEGs in high-pyroptosis group (Fig. 4E). The results of GO and KEGG analysis indicated that 152 overlapping DEGs mainly regulated the recruitment and viability of immune cells by regulating classical signaling pathways including TNF pathway and NF-kappa B pathway, thereby accelerating the progression of GC (Fig. 4F). Therefore, these 152 overlapping DEGs were chosen to further analysis.

3.4. Construction and validation of prognostic models based on PRGs

Univariate Cox analysis was first utilized to screen the values of 152 overlapping DEGs for the prognostic prediction of GC patients. Then, LASSO and multivariate Cox analysis were used to screen out the 6 prominent genes (*C12orf75*, *VCAN*, *RGS2*, *MKNK2*, *SOCS3* and *TNFAIP2*), and calculate the coefficient of each gene in formula of risk score (Figs. 5A and 5B). Risk score $= (0.135316 \times$ *VCAN*$) + (-0.29069 \times$ *MKNK2*$) + (0.148085 \times$ *RGS2*$) + (0.185646 \times$ *SOCS3*$) + (-0.2081 \times$ *TNFAIP2*$) + (0.166387 \times$ *C12orf75*). We also analyzed the correlation of each gene with GC prognosis and plotted KM curves, finding that all six genes are related to prognosis of patients (Fig. S4). Subsequently, GC patients were classified into two groups on the basis of the median value of all patients' risk scores. The heatmap displayed the expression of *C12orf75*, *VCAN*, *RGS2*, *MKNK2*, *SOCS3* and *TNFAIP2* in two groups (Fig. 5C). As shown in Figs. 5D and 5E, the proportion of death was higher in the GC patients with higher risk scores. In addition, patients with higher risk scores had shorter long-term survival time compared with patients with lower risk scores by using Kaplan-Meier survival analysis (Fig. 5F). Then, the risk signature was utilized to predict the long-term survival probability of GC patients. The accuracy of signature for the predictive probability of 1-, 3- and 5-year all outstripped 0.65 in GC (Fig. 5G). A nomogram comprised of risk signature and various clinicopathological features was successfully constructed to predict the survival time of GC patients (Fig. 5H). The validity and accuracy of the nomogram for the predictive probability of 1-, 3- and 5-year were validated through calibration curve (Fig. 5I). Further, a webserver (https://pumc.shinyapps.io/GastricCancer/) was constructed to make full use of the nomogram in prognostic prediction for GC patients. The quick response code provided a convenient entrance using the online tool in clinical practice for physicians (Fig. 5J). For the rigor of this study, the Asian Cancer Research Group (ACRG) cohort (GSE62254) was utilized to validate the clinical values of signature. The signature not only well distinguished the OS and DFS between the two groups, but also precisely forecasted the 1-, 3-, and 5-year OS and DFS of GC patients (Figs. 5K and 5L). In summary, we preliminarily investigated and validated the direction and value of using PRGs to predict the prognosis of GC patients in clinical translation.

3.5. GSEA and functional enrichment analyses

The significance of survival time in the two groups meant that there was a great heterogeneity of the genome between them. GSEA analysis was used to clarify the underlying mechanisms in two groups (Table S3). As shown in Figs. 6A and 6B, classical signaling pathways were involved in the high-risk group, including activation of cell cycle and oxidative phosphorylation and inhibition of MAPK pathway, JAK-STAT pathway, TGF-β pathway, PD-1 signaling, Ecm receptor interaction, focal adhesion, cell adhesion molecules cams, cytokine cytokine receptor interactior and pathways in cancer. In addition, the results of GO analysis also proved that DEGs in two groups greatly regulated the biological process and various cell functions to aggravate the tumor development (Figs. 6C and 6E). The data of KEGG analysis validated the profound effects of DEGs in two groups on these critical signaling pathways (Figs. 6D and 6F), which was finally reflected in the prognostic disparity between the two groups of GC patients.

3.6. Estimation of tumor immune microenvironment

The relationship of tumor immune microenvironment and risk signature was also investigated. As shown in Fig. 7A, the risk scores were negatively related to the immune clearance, while positively related to the immunosuppression of various immune cells, such as $CD8^+$ T cells decreased with the risk scores increased. Furthermore, the results of correlation between the 6 PRGs and immune cells were presented in the Fig. 7B. VCAN was mainly positive correlations to M2 macrophages and negative correlations to the activation of dendritic cells. While *C12orf75* and *TNFAIP2* were mainly positive correlations to M0 and M1 macrophages. *RGS2* was a positive correlation to mast cells resting. And *MKNK2* was negative correlations to activation of mast cells. *SOCS3* was negative to function of memory B cells. The data revealed that the 6 PRGs that constructed the risk signature profoundly regulated the immune microenvironment of GC. The somatic mutation profile was

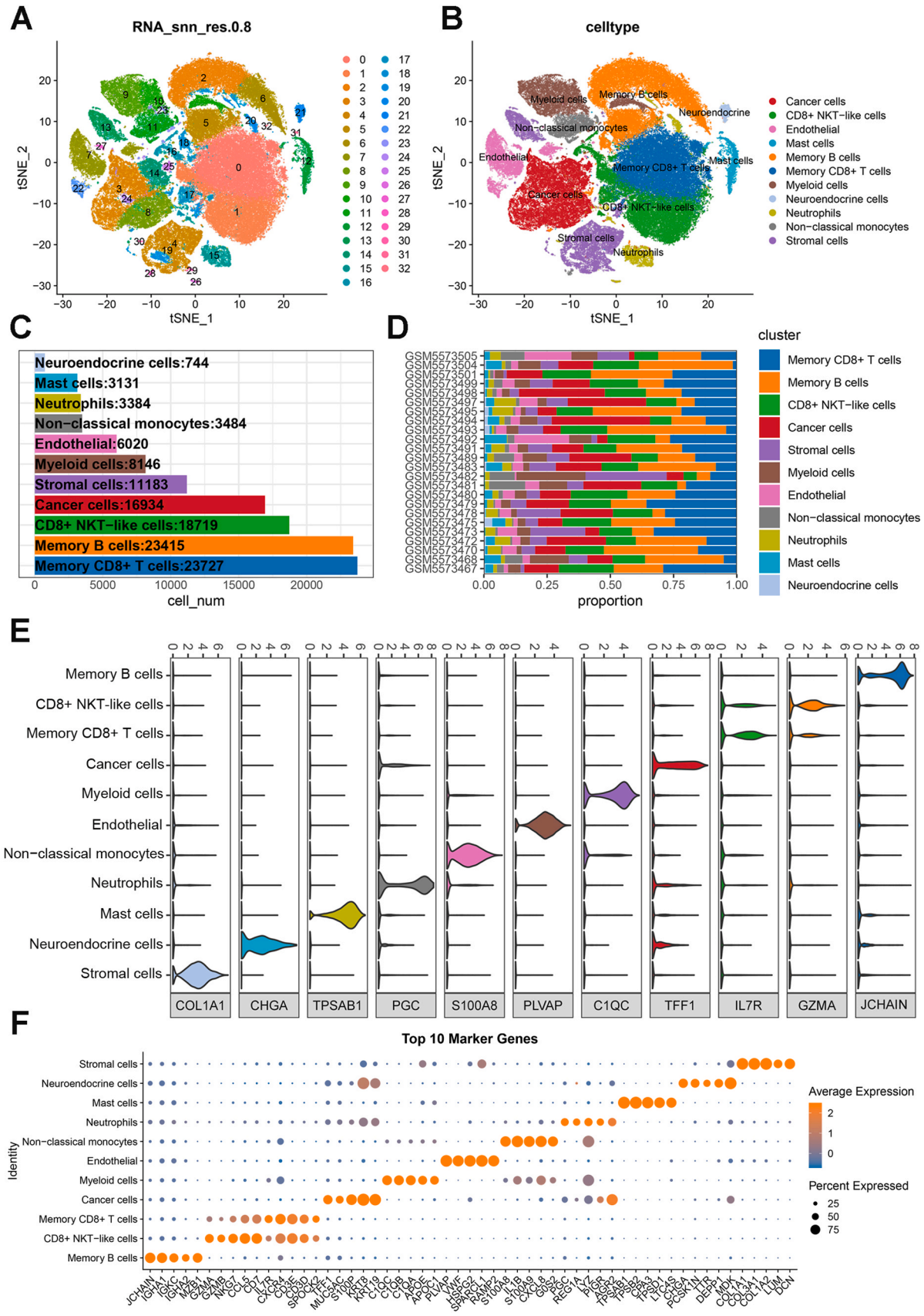

Fig. 2. Identification of cell type by scRNA-seq analysis. A T-SNE distribution of 32 independent cell clusters. B T-SNE distribution of cell types identified by marker genes. C The total number of each cell type identified by marker genes. D The distribution of cell types in different specimens. E Violin plots represent the expression levels of the marker genes for the eleven cell types. F Bubble diagram shows the top 10 marker genes in each annotated cell types.

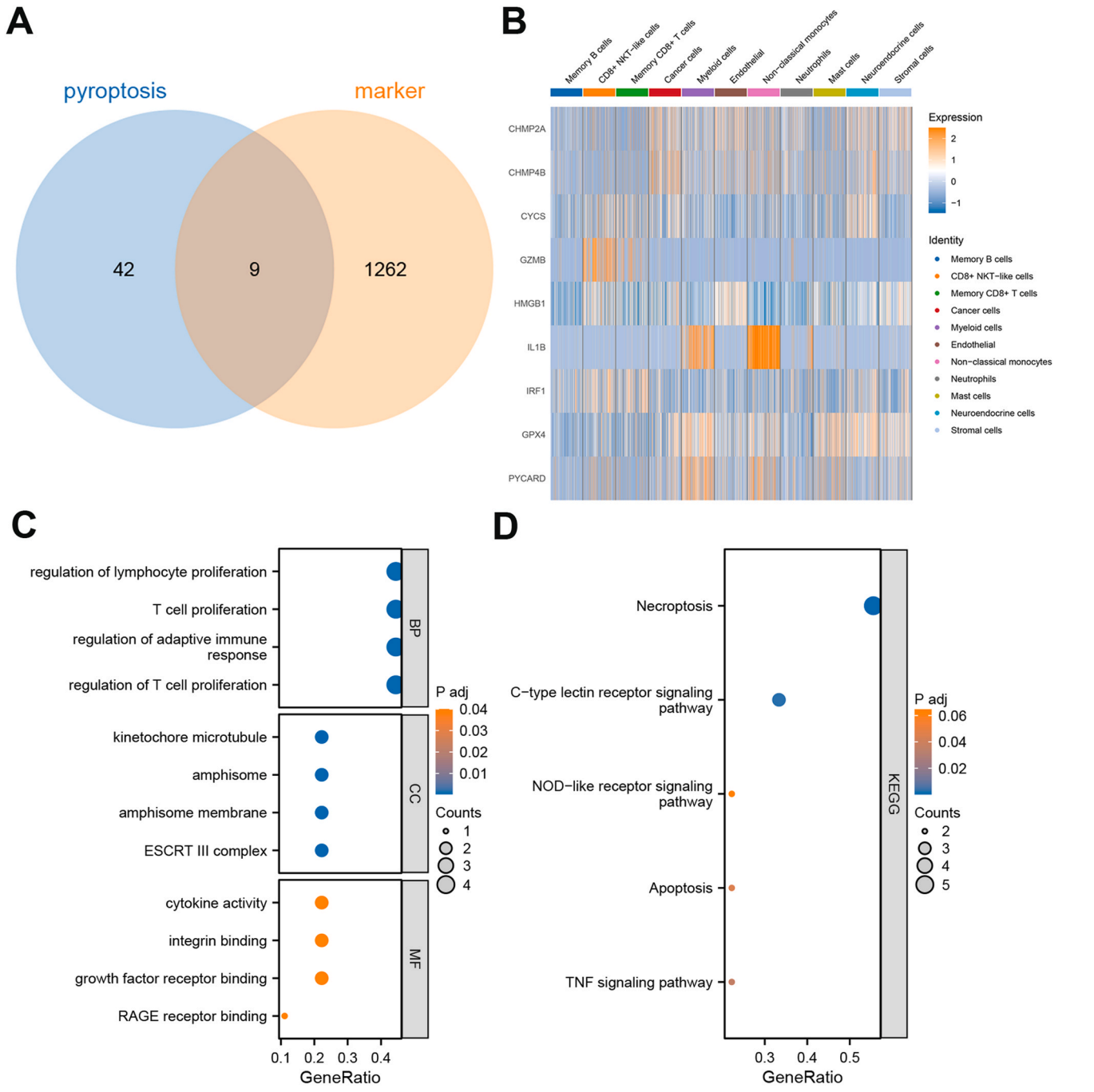

Fig. 3. Differentially expressed pyroptosis-related genes (PRGs) in gastric cancer at single cell level. A Venn diagram of differentially expressed PRGs and marker genes. B Heatmap showed the expression of 9 PRGs in each annotated cell types. C The GO analysis of the differentially expressed PRGs. D The KEGG analysis of the differentially expressed PRGs.

detected in the total samples and two groups. From the integrated samples, the *TTN*, *TP53*, *MUC16*, *ARID1A* and *LRP1B* were the top five frequently mutated genes (FMGs) in GC (Fig. S5A). *TTN* and *TP53* were both the top two FMG in two groups. However, the *MUC16*, *ARID1A* and *CSMD3* were the resting three FMG of top five in high-risk group (Fig. S5B). *LRP1B*, *MUC16* and *SYNE1* were the FMG of top five in low-risk group (Fig. S5C).

3.7. The clinical application of risk signature in GC

Lack of typical symptoms and the low prevalence of screening result in a low diagnosis rate of early-stage GC in China [2]. This phenomenon warranted postoperative adjuvant chemotherapy and the use of immune checkpoint inhibitors (ICIs) for comprehensive treatment. Patients with low risk scores were often good response to 5 −Fluorouracil, lapatinib, methotrexate and paclitaxel. While patients with high risk scores were more sensitive to cisplatin treatment (Fig. 8A). In addition, the increasing expression of *VCAN*, *MKNK2*, *SOCS3* and *TNFAIP2* often meant the elevation of *CD274* in GC (Fig. 8B). Similarly, the *BTLA*, *VSIR*, *CD200*, *CD200R1*, *CD244*, *CD276*, *CD28*, *CD40*, *CD40LG*, *CD48*, *CD80*, *CD86*, *HAVCR2*, *ICOS*, *LAIR1*, *NRP1*, *PDCD1LG2*, *TNFRSF4*, *TNFRSF8*, *TNFRSF9*, *TNFSF14*, *TNFSF18* and *TNFSF4* were significantly

Table 1
The results of Venn diagram between differentially expressed genes in diverse cell types and pyroptosis-related genes.

Ontology	ID	Description	GeneRatio	BgRatio	pvalue	p.adjust
BP	GO:0042129	regulation of T cell proliferation	4/9	174/18800	8.61e-07	0.0004
BP	GO:0002819	regulation of adaptive immune response	4/9	188/18800	1.17e-06	0.0004
BP	GO:0042098	T cell proliferation	4/9	204/18800	1.63e-06	0.0004
CC	GO:0000815	ESCRT III complex	2/9	11/19594	1.03e-05	0.0003
CC	GO:1904930	amphisome membrane	2/9	11/19594	1.03e-05	0.0003
CC	GO:0044753	amphisome	2/9	13/19594	1.46e-05	0.0003
MF	GO:0070851	growth factor receptor binding	2/9	139/18410	0.0020	0.0400
MF	GO:0005178	integrin binding	2/9	156/18410	0.0025	0.0400
MF	GO:0050786	RAGE receptor binding	1/9	10/18410	0.0049	0.0400
KEGG	hsa04217	Necroptosis	5/9	159/8164	3.11e-07	2.34e-05
KEGG	hsa04625	C-type lectin receptor signaling pathway	3/9	104/8164	0.0002	0.0030
KEGG	hsa04668	TNF signaling pathway	2/9	112/8164	0.0063	0.0364
KEGG	hsa04210	Apoptosis	2/9	136/8164	0.0092	0.0449
KEGG	hsa04621	NOD-like receptor signaling pathway	2/9	184/8164	0.0164	0.0647

upregulated in high-risk group, while *LGALS9*, *TNFRSF14* and *TNFRSF18* were increased in low-risk group (Fig. 8C). The above data revealed that the risk signature contained 6 PRGs can be used to guide the therapy selection for GC patients in the foreseeable future.

3.8. Validation of PRGs in specimens and its correlation with immune cell infiltrations in GC

We detected the expression of *VCAN*, *TNFAIP2*, *RGS2*, *MKNK2*, *SOCS3* and *C12orf75* in the GC by using tissue array. As shown in Figs. 9A and 9B, *VCAN*, *TNFAIP2* and *SOCS3* were greatly elevated in the GC tissues while *RGS2* and *MKNK2* were decreased in the tumor samples via IHC staining. There was no significant difference in *C12orf75* between GC tissues and adjacent tissues, probably due to the limited number of samples (Fig. 9A). Further, by integrating the clinical information of the sample and the data on PRGs' expression, we found that patients with higher expressions of *VCAN* frequently predicted worse T and AJCC stage; higher expression of *TNFAIP2* and *SOCS3* usually meant worse AJCC stage; lower expressions of *MKNK2* often forecasted worse T stage and advanced clinical stage and lower expressions of *RGS2* generally signified worse AJCC stage of GC (Table 2). The close relationships between 5 PRGs and clinicopathological characteristics also verified the logic and accuracy of the pyroptosis-related signature in predicting the survival time of GC patients. As the abovementioned exploration of the potential relationship between PRGs and immune cell infiltrations, we simultaneously detected the infiltrations of regulatory T cells (Tregs) (*FoxP3*) and M2 type of tumor-associated macrophages (TAMs) (*CD163*) and the expression of *CD274* in tumor cells in tissue microarray. The results indicated that *VCAN* was positively related to the infiltrations of Tregs and M2 TAMs in GC TME and the expression of *CD274* in tumor cells (Figs. 9C and 9D). However, *TNFAIP2*, *RGS2*, *MKNK2*, *SOCS3* and *C12orf75* were not significantly associated with the Tregs and M2 TAMs in TME and the expression of CD274. The abovementioned data not only demonstrated that PRGs are closely related to the clinicopathology of GC patients but also that high expression of *VCAN* is positive to the immunosuppressive TME of GC.

4. Discussion

Cell pyroptosis characterized by inflammasome is a Gasdermin-dependent programmed cell death and can release plenty of inflammatory factors to cause inflammatory responses [9,29]. The role of cell pyroptosis in tumors is complex and dynamic [30,31]. On the one hand, inflammasomes can induce pyroptosis of tumor cells and inflammatory response, thereby inhibiting the proliferation of tumor cells. On the other hand, the cumulative effect of inflammasomes can also form an appropriate TME for tumor cells and exert a role in promoting tumor progression. Therefore, the function of cell pyroptosis in the development of GC needs to be urgently explored.

GC is the most common malignant tumor of the digestive system, which seriously threatens human health [1,32]. Its incidence is closely related to *Helicobacter pylori* infection, heredity, high nitrite diet, environmental pollution and other factors [33]. The lack of typical symptoms and the low prevalence of screening result in a low diagnosis rate of early-stage GC (about 10%) [34]. At the same time, there is a lack of biomarkers related to treatment response and prognostic predictions, and the survival time of patients is dismal [35]. Nowadays, with the in-depth investigation of oncogene sequence and pathogenesis, gene-based targeted precision medicine has become the primary treatment for GC, especially for advanced and recurrent GC [36,37]. Hence, the identification of effective biomarkers is crucial to boost the accuracy of prognostic prediction and to select the sensitive treatment strategies for GC patients.

scRNA-seq is a cutting-edge technology that reveals the transcriptome alterations of cells at the single cell level. It has unique advantages in exploring the heterogeneity of cell populations and exploring cell types related to tumorigenesis, development and metastasis [15,16]. GC-related cells with different molecular markers were clustered by scRNA-seq to identify subgroups that may be associated with poor prognosis and drug resistance in patients [16]. In the exploration of TME, it is possible to ascertain immune cell subsets related to immune evasion and identify novel promising immunotherapy targets in GC [17]. The rapid development of scRNA-seq enables researchers to better understand the heterogeneity of cells in GC and elucidate the complex mechanisms of tumor development and metastasis, providing new perspectives for establishing precise treatment strategies for GC. The aforementioned facts demonstrated the clinical significance of utilizing scRNA-seq and transcriptome RNA-seq to investigate the underlying mechanism of cell pyroptosis in GC and identify powerful biomarkers to predict prognosis and treatment response in GC.

The scRNA-seq data from 24 GC patients was obtained from GSE183904 dataset after strictly screening with quality control. 33 cell clusters were successfully classified into 11 cell types after annotation. Then, 9 overlapping differentially expressed PRGs between the PRGs and marker genes were selected to further detect at the single-cell level in GC. *CHMP2A* and *CHMP4B* were specifically enriched in the cancer cells and may also exert critical roles in GC in addition to other tumors [38–41]. The results of enrichment analysis validated the hypothesis that 9 differentially expressed PRGs had effects on signal transduction and functional alterations of GC. Due to the critical roles of 9 differentially expressed PRGs in tumor progression, we scored each cell based on the expression of 9 PRGs. In this study, our primary focus was on comparing pyroptosis scenarios among different cell types in gastric cancer tissues, with an emphasis on the pyroptosis states of cell groups. Moving forward, we intend to extend our focus to the pyroptosis conditions of individual cells within each cell population in the future. The 1209 DEGs in high-pyroptosis group were screened through comparing with the low-pyroptosis group. Next, 152 overlapping DEGs were

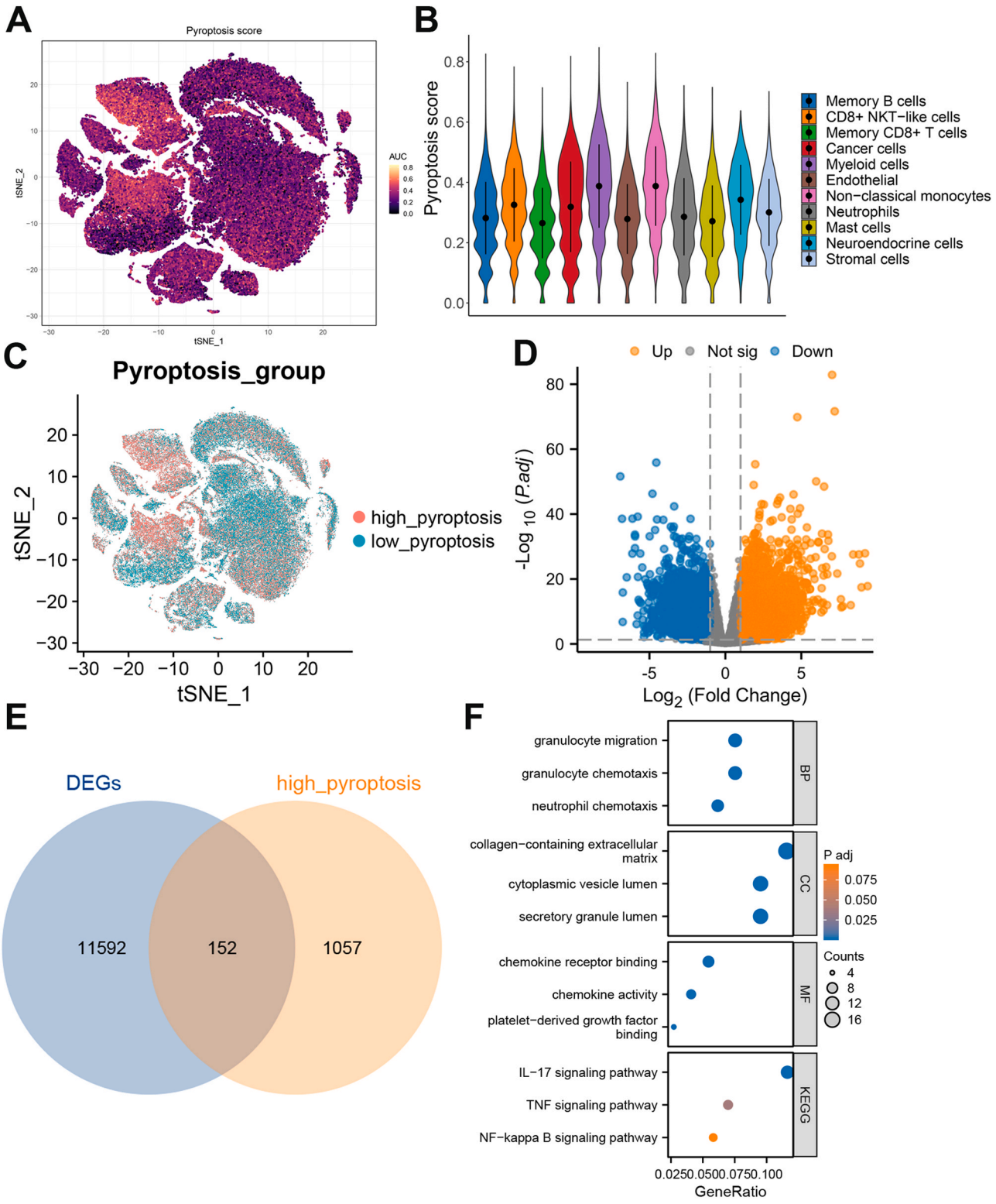

Fig. 4. Scoring the cell type based on the expression of PRGs. A T-SNE distribution of pyroptosis score of cells by using AUCell function. B Violin plots of pyroptosis score of cell type. C T-SNE distribution of high-pyroptosis and low-pyroptosis group. D Volcanic plot of differentially expressed genes (DEGs) between GC and adjacent tissues. E Venn diagram of DEGs between GC and adjacent tissues and specifically expressed genes in high-pyroptosis group. **F** The results of GO and KEGG analysis of DEGs in high-pyroptosis group.

obtained after integrating the DEGs between the GC and adjacent normal tissues and 1209 DEGs in the high-pyroptosis group. These 152 overlapping DEGs were the panel to establish a pyroptosis-related signature. Univariate Cox, LASSO and multivariate Cox analysis were utilized to screen out the 6 prominent genes (*C12orf75*, *VCAN*, *RGS2*, *MKNK2*, *SOCS3* and *TNFAIP2*) and construct the risk score formula. GC patients were classified into two groups on the basis of the median value of all patients' risk scores. Furthermore, the signature well distinguished the survival disparity between the two groups of GC patients and remedied the limitations of the clinical practice of TNM staging [42]. In

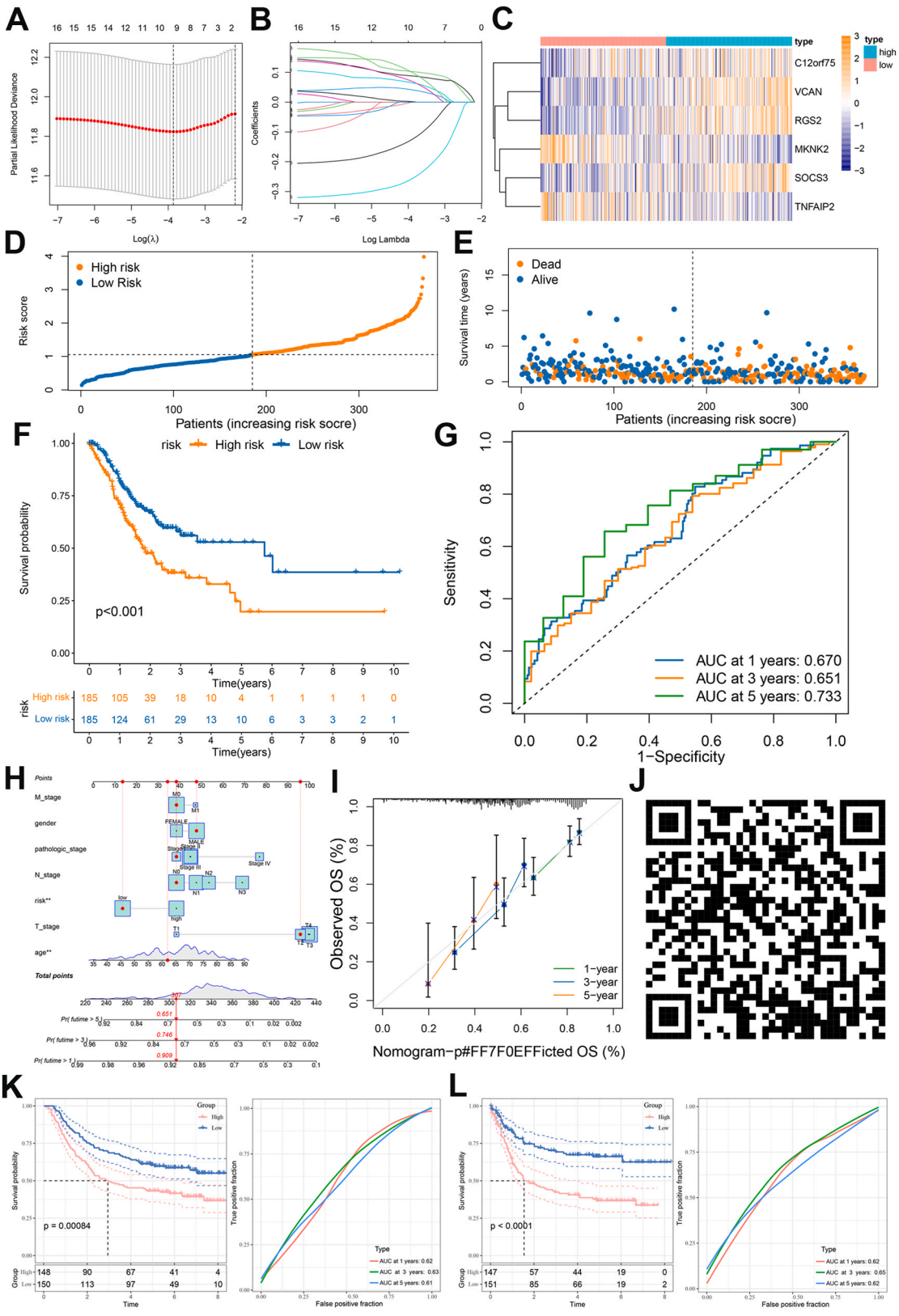

Fig. 5. Construction and validation of prognostic models based on PRGs. A LASSO Cox regression analysis of the association between deviance and log(λ). B LASSO Cox regression analysis of the association between coefficients of genes and log(λ). C Heatmap showed the differences of 6 PRGs between high risk and low risk patients. D The survival status of GC patients ranked by risk score. E The survival time of GC patients ranked by risk score. F Kaplan-Meier analysis between high-risk groups and low-risk groups. G Time-dependent ROC curve of risk score predicting the 1-, 3-, and 5-year overall survival (OS). H Details of the nomogram. I The calibration curve for predicting 1-, 3-, and 5-year OS. J The quick response code of online dynamic nomogram K The OS discrepancy between the high-risk and low-risk groups and the ROC curve of risk score predicting the 1-, 3-, and 5-year OS using the GSE62254 dataset. L The DFS discrepancy between the high-risk and low-risk groups and the ROC curve of risk score predicting the 1-, 3-, and 5-year DFS using the GSE62254 dataset.

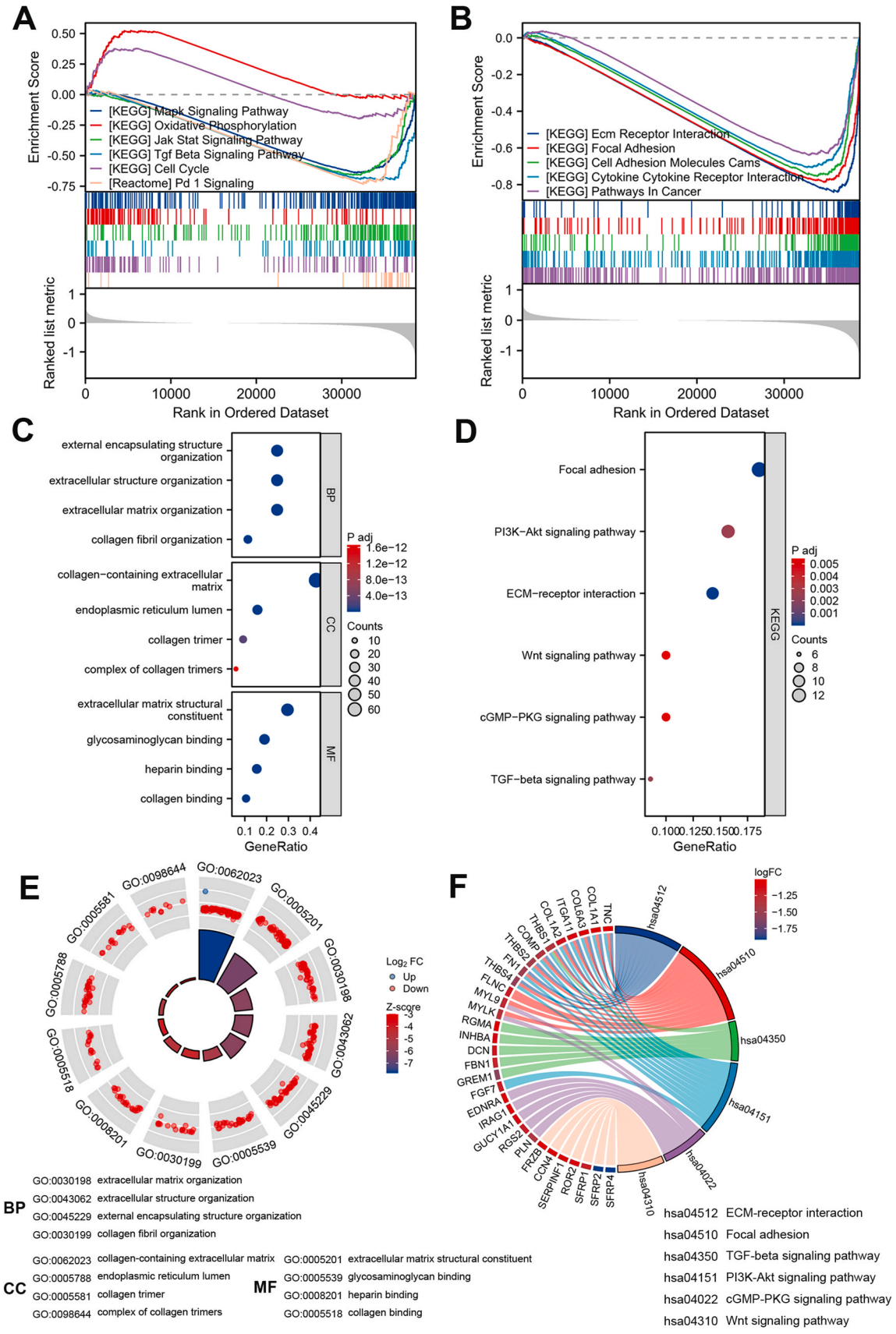

Fig. 6. GSEA analysis and enrichment analyses of differentially expressed genes between high-risk groups and low-risk groups. A-B The GSEA analysis of differentially expressed genes between high-risk groups and low-risk groups. C The results of GO analysis. D The results of KEGG analysis. E The results of GO analysis. **F** The results of KEGG analysis.

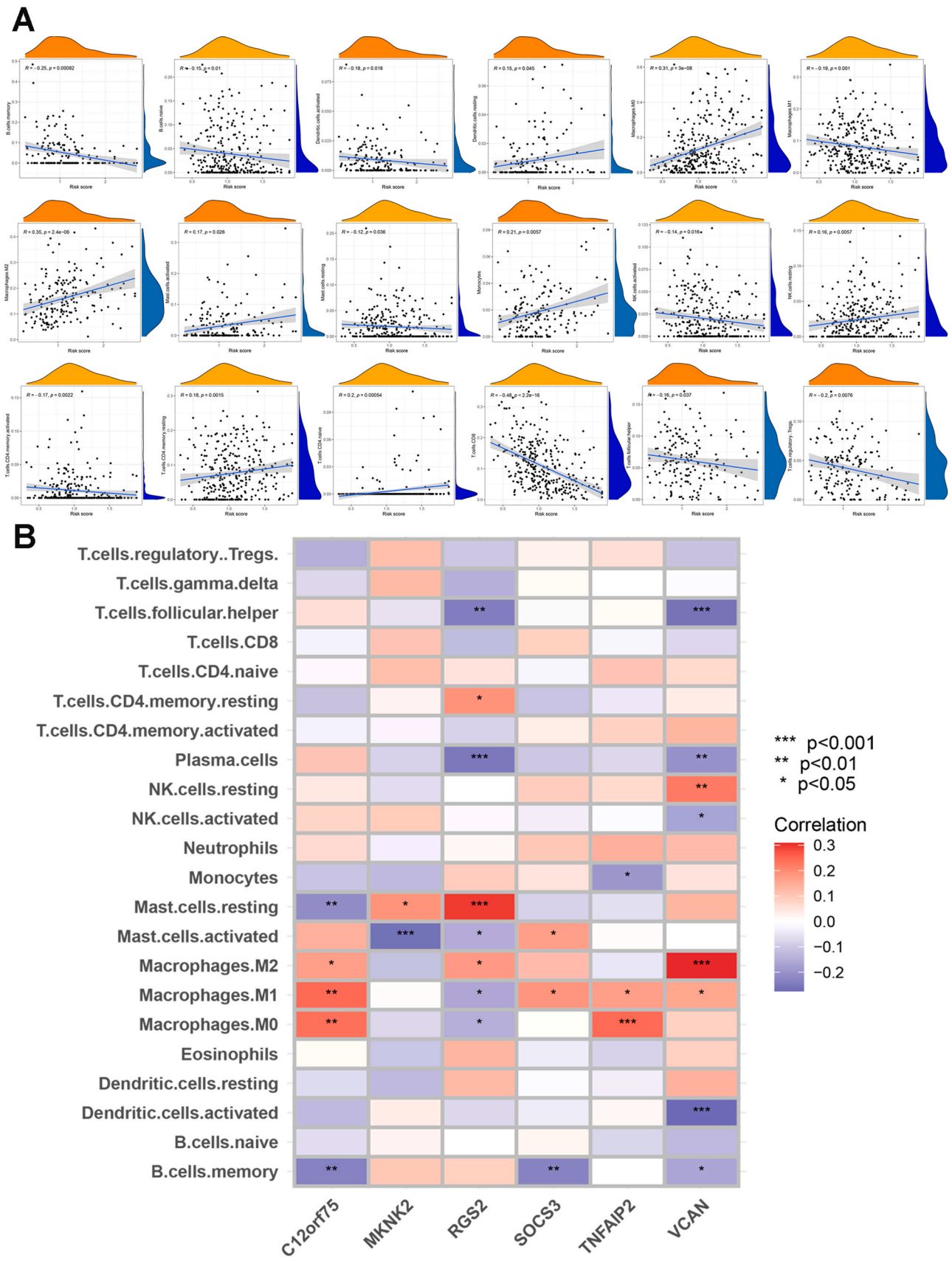

Fig. 7. The correlation between the risk signature and tumor immune microenvironment. A The correlation between the risk score and infiltrated immune cells. **B** The correlation between the 6 PRGs and infiltrated immune cells.

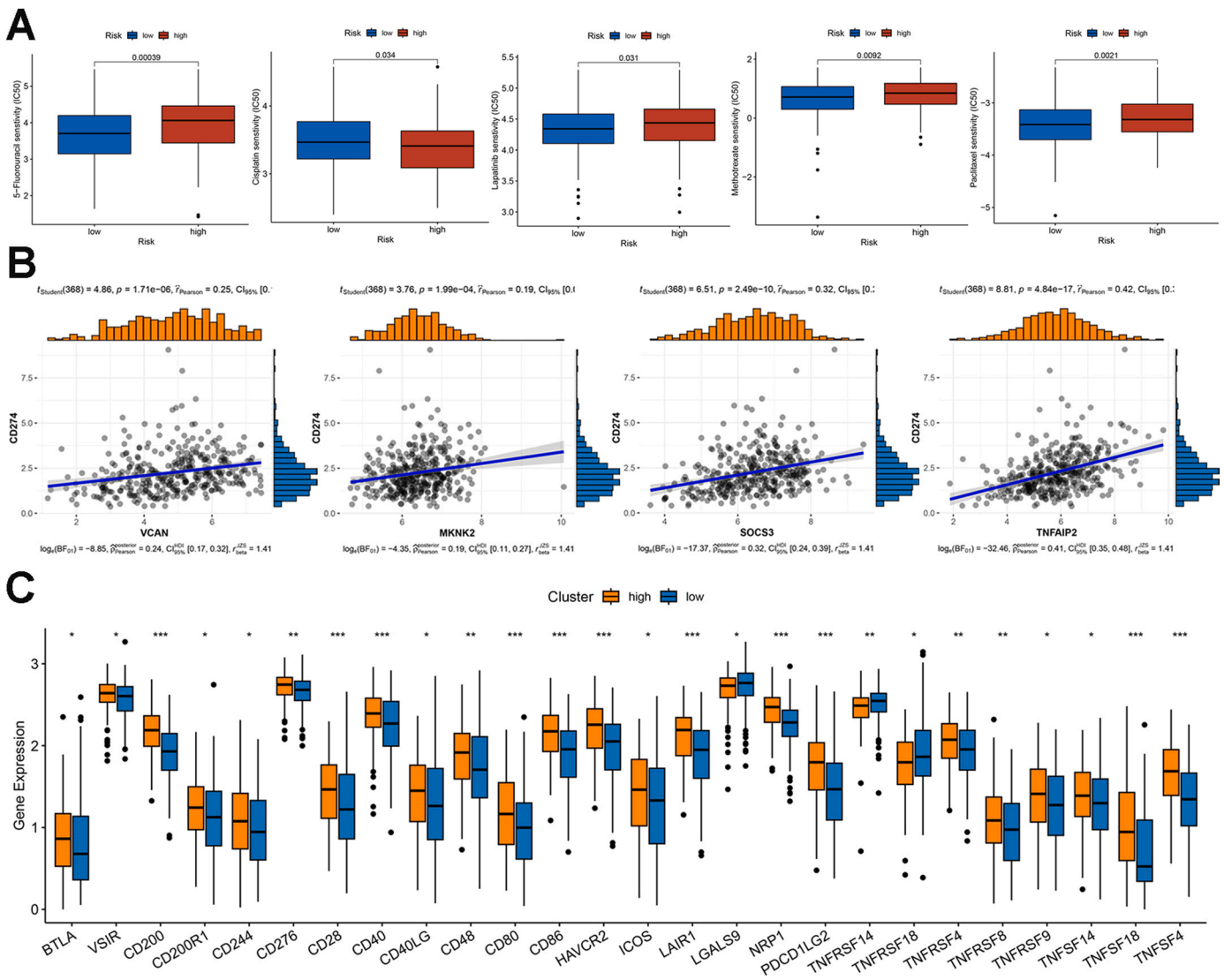

Fig. 8. Drug sensitivity and immune infiltration level analysis based on the risk model. A The results of drug sensitivity analysis between high-risk and low-risk groups. B The correlation between the PRGs and CD274. C The expression of immune checkpoints between high-risk and low-risk groups.

addition, an online tool was built to help physicians more easily predict the survival probability of GC patients in clinical practice. The discrepancy in the activation and inhibition of signal pathways explained the differences in the survival time between the two groups at the molecular mechanism level. In addition, high risk scores often indicated an immunosuppressive TME for promoting tumor progression whereas low risk scores meant an unfavorable TME for repressing tumor development. The discrepancy in the mutation profile between the two groups can be used to guide the treatment methods and drug selection for GC patients. As the aforementioned data, chemotherapy was essential for advanced-stage GC patients who accounted for a high proportion of China [2]. Nowadays, the emergence of ICIs represented by PD-L1 was the first-line treatment for advanced-stage GC patients, but only a few patients can benefit from the treatment of ICIs [4,43]. Fortunately, this signature can be exploited to guide the selection of sensitive chemotherapy drugs and appropriate ICIs for GC patients, thereby increasing the survival time of patients. For the rigor and accuracy of the study, we detected the expression of *VCAN*, *TNFAIP2*, *RGS2*, *MKNK2*, *SOCS3* and *C12orf75* in 54 paired GC tissues and adjacent normal tissues by IHC staining. Consistent with the transcriptome expression in the TCGA database, *VCAN*, *TNFAIP2* and *SOCS3* were greatly elevated in the GC tissues while *RGS2* and *MKNK2* were decreased in the tumor samples. Besides, the expression level of each PRG was closely related to the clinical pathological characteristics of GC patients. Abundant studies have demonstrated that immunosuppressive TME was an indispensable factor in immune evasion and malignant progression of tumor cells. When PD-L1 on the surface of tumor cells binds to PD-1 on T cells, the proliferation and function of T cells are inhibited, thereby negatively regulating the anti-tumor immune response and escaping from immune clearance [44]. The critical role of TAMs was widely investigated in GC progression [45]. M2 TAMs have been reported to significantly enhance malignant development and immune evasion of GC. Tregs are one of the $CD4^+$ T cells, which can inhibit the inflammatory response of TME by inhibiting the function and migration of immune cells, secreting inhibitory cytokines and destroying metabolism [46]. Xia et al. found that *VCAN* was indirectly positively correlated with more infiltrations of $CD8^+$ T cells in melanoma [47]. Further, *VCAN* was reported to be elevated in GC tissues and enhance cell proliferation and metastasis of GC [48]. Nevertheless, the correlation between *VCAN* and immune cell infiltrations in GC TME remains blank. Hence, we try to explore the potential relationship between PRGs and immune cell infiltrations in GC TME. Surprisingly, tissues with high expression of *VCAN* frequently presented high expression of *CD274*, *CD163* and *FoxP3*, which meant a potential correlation between *VCAN* and *CD274*, M2 TAMs and Tregs in

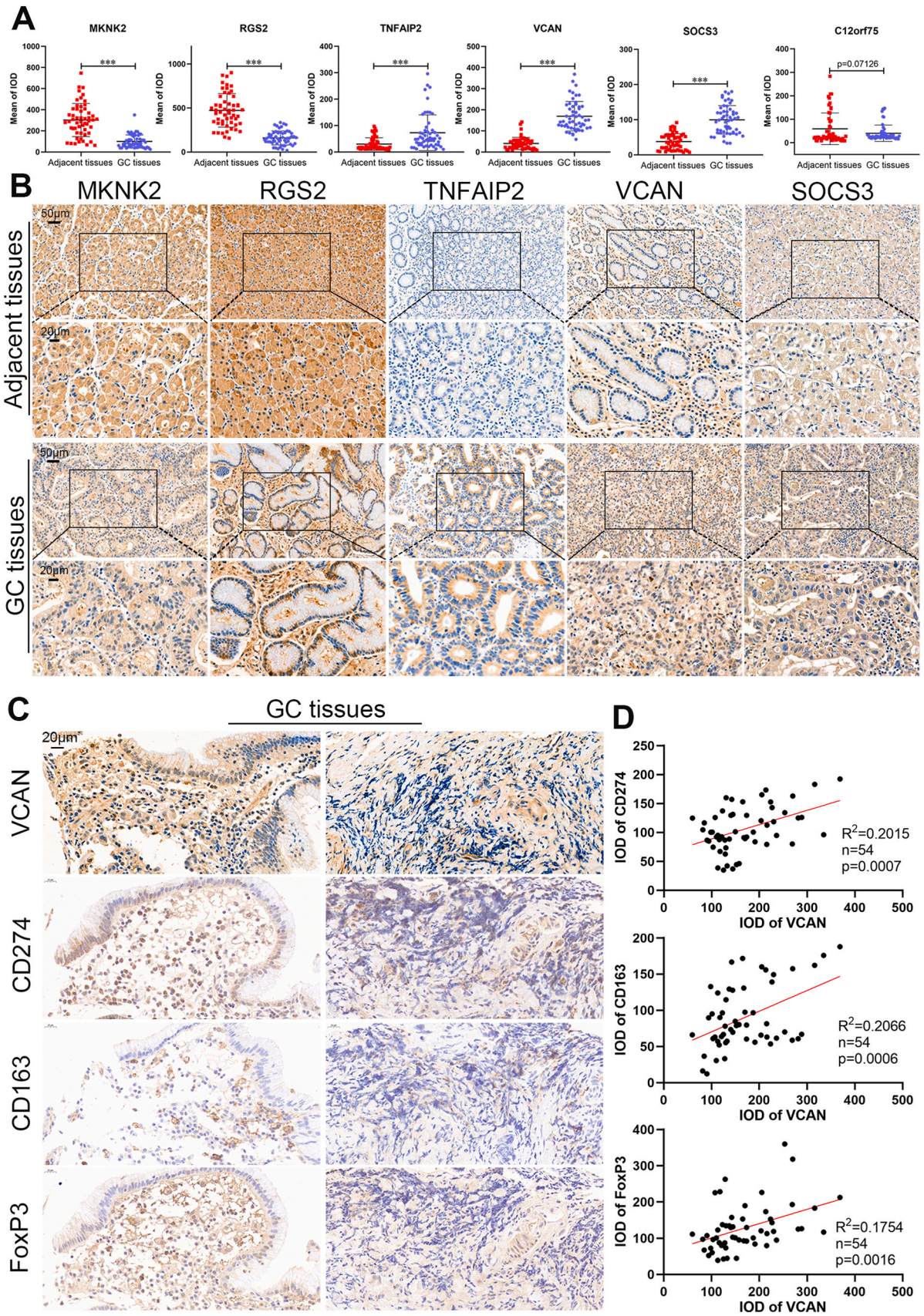

Fig. 9. The expression of MKNK2, RGS2, TNFAIP2, VCAN, SOCS3, C12orf75, CD274, CD163 and FoxP3 in GC. A The expression of MKNK2, RGS2, TNFAIP2, VCAN, SOCS3 and C12orf75 in 54 paired GC and adjacent normal tissues. B The representative IHC images of MKNK2, RGS2, TNFAIP2, VCAN and SOCS3 in GC and adjacent normal tissues (scale bar: 50 μm and 20 μm). C The representative IHC images of VCAN, CD274, CD163 and FoxP3 in the same GC tissues (scale bar: 20 μm). D The correlation between VCAN and CD274, CD163 and FoxP3 in the GC tissues. Student's t-test was used to determine statistical significance: * ** $p < 0.001$.

Table 2
Relationship between clinicopathological characteristics and expression of MKNK2, RGS2, TNFAIP2, VCAN and SOCS3 in gastric cancer (n = 54).

	Expression of MKNK2		Expression of RGS2		Expression of TNFAIP2		Expression of VCAN		Expression of SOCS3	
	High (n = 27)	Low (n = 27)	High (n = 27)	Low (n = 27)	High (n = 27)	Low (n = 27)	High (n = 27)	Low (n = 27)	High (n = 27)	Low (n = 27)
Gender										
Male	19	16	18	17	15	20	17	18	18	17
Female	8	11	9	10	12	7	10	9	9	10
Age (years)										
< 55	5	5	7	3	5	5	5	5	4	6
≥ 55	22	22	20	24	22	22	22	22	19	29
Tumor location										
Fundus	6	5	6	5	5	6	6	5	7	4
Body	14	11	10	15	13	12	14	11	12	13
Antrum	7	11	11	7	9	9	7	11	8	10
Tumor size (cm)										
< 3	**20**	**11**	14	17	14	17	13	18	12	19
≥ 3	**7**	**16** *	13	10	13	10	14	9	15	8
Tumor T stage										
1 + 2	21	16	20	17	18	19	**15**	**22**	16	21
3 + 4	6	11	7	10	9	8	**12**	**5** *	11	6
Tumor N stage										
0 + 1	22	16	21	17	17	21	17	21	14	24
2 + 3	5	11	6	10	10	6	10	6	13	3
AJCC stage										
I + II	**25**	**16**	**24**	**17**	**17**	**24**	**17**	**24**	**16**	**25**
III + IV	**2**	**11** * *	**3**	**10** *	**10**	**3** *	**10**	**3** *	**11**	**2** * *
Differentiation										
Well-moderately	10	5	7	8	9	6	7	8	9	6
Poorly	17	22	20	19	18	21	20	19	18	21

Statistical significance was determined by the chi-square test. (*p < 0.05, **p < 0.01).

GC TME. VCAN would be a potent target in immunotherapy by reversing the immunosuppressive TME of GC. Additionally, *in vivo* and *in vitro* experiments and exploration of molecular mechanisms of PRGs in GC need to be gradually implemented.

5. Conclusions

In summary, we constructed a pyroptosis-related signature to potently predict the survival time and treatment response of GC by integrating scRNA-seq and transcriptome RNA-seq data. This study may guide the research orientation of cell pyroptosis in GC, the selection of chemotherapy drugs and ICIs for patients and VCAN as a potential target of immunotherapy in the future.

Authors' contributions

JL and TY conceptualized the research, downloaded and analyzed the data. TY built up the webserver. JS and MWM produced the figures. ZCZ and XY wrote the manuscript. WMK and XY supervised and revised the manuscript.

Funding

This study was funded by the National High Level Hospital Clinical Research Funding (2022-PUMCH-C-048, 2022-PUMCH-B-005, 2022-PUMCH-A-051), Beijing Natural Science Foundation (7232117), Beijing Medical Award Foundation (YXJL-2021-0838-0761 (WCJZL202106), Wu Jieping Medical Foundation (320.6750.2022-10-1) and Beijing Xisike Clinical Oncology Research Foundation (Y-NESTLE2022ZD-0105).

CRediT authorship contribution statement

Jie Li: Conceptualization, Visualization, Writing – original draft. **Tian Yu**: Data curation, Software, Visualization, Writing – review & editing. **Juan Sun**: Validation, Investigation, Writing – review & editing. **Mingwei Ma**: Formal Analysis, Validation, Writing – review & editing. **Zicheng Zheng**: Validation, Investigation, Writing – review & editing. **Weiming Kang**: Funding acquisition, Supervision, Writing – review & editing, Project administration. **Xin Ye**: Funding acquisition, Supervision, Writing – review & editing.

Declaration of Competing Interest

The authors declare that they have no known competing financial interests or personal relationships that could have appeared to influence the work reported in this paper.

Acknowledgments

None.

Appendix A. Supporting information

Supplementary data associated with this article can be found in the online version at doi:10.1016/j.csbj.2024.02.002.

References

[1] Sung H, Ferlay J, Siegel RL, et al. Global cancer statistics 2020: GLOBOCAN estimates of incidence and mortality worldwide for 36 cancers in 185 countries. CA: a Cancer J Clin 2021;71(3):209–49.
[2] Zheng R, Zhang S, Zeng H, et al. Cancer incidence and mortality in China, 2016. J Natl Cancer Cent 2022.
[3] Johnston FM, Beckman M. Updates on management of gastric cancer. Curr Oncol Rep 2019;21(8):67.
[4] Janjigian YY, Shitara K, Moehler M, et al. First-line nivolumab plus chemotherapy versus chemotherapy alone for advanced gastric, gastro-oesophageal junction, and oesophageal adenocarcinoma (CheckMate 649): a randomised, open-label, phase 3 trial. Lancet (Lond, Engl) 2021;398(10294):27–40.
[5] Bang YJ, Van Cutsem E, Fuchs CS, et al. KEYNOTE-585: phase III study of perioperative chemotherapy with or without pembrolizumab for gastric cancer. Future Oncol (Lond, Engl) 2019;15(9):943–52.
[6] Li J, Yu T, Sun J, et al. Comprehensive analysis of cuproptosis-related immune biomarker signature to enhance prognostic accuracy in gastric cancer. Aging 2023; 15(7):2772–96.

[7] Li J, Feng Y, Heng D, et al. Circulating non-coding RNA cluster predicted the tumorigenesis and development of colorectal carcinoma. Aging 2020;12(22):23047–66.
[8] Rühl S, Shkarina K, Demarco B, Heilig R, Santos JC, Broz P. ESCRT-dependent membrane repair negatively regulates pyroptosis downstream of GSDMD activation. Sci (N Y, NY) 2018;362(6417):956–60.
[9] Shi J, Zhao Y, Wang K, et al. Cleavage of GSDMD by inflammatory caspases determines pyroptotic cell death. Nature 2015;526(7575):660–5.
[10] Ding J, Wang K, Liu W, et al. Pore-forming activity and structural autoinhibition of the gasdermin family. Nature 2016;535(7610):111–6.
[11] Gao YL, Zhai JH, Chai YF. Recent advances in the molecular mechanisms underlying pyroptosis in sepsis. Mediat Inflamm 2018;2018:5823823.
[12] Bartoli-Leonard F, Zimmer J, Sonawane AR, et al. NLRP3 inflammasome activation in peripheral arterial disease. J Am Heart Assoc 2023;12(6):e026945.
[13] Feng WQ, Zhang YC, Xu ZQ, et al. IL-17A-mediated mitochondrial dysfunction induces pyroptosis in colorectal cancer cells and promotes CD8 + T-cell tumour infiltration. J Transl Med 2023;21(1):335.
[14] Dai J, Qu T, Yin D, et al. LncRNA LINC00969 promotes acquired gefitinib resistance by epigenetically suppressing of NLRP3 at transcriptional and posttranscriptional levels to inhibit pyroptosis in lung cancer. Cell death Dis 2023;14(5):312.
[15] Li L, Xiong F, Wang Y, et al. What are the applications of single-cell RNA sequencing in cancer research: a systematic review. J Exp Clin Cancer Res: CR 2021;40(1):163.
[16] Deng G, Zhang X, Chen Y, et al. Single-cell transcriptome sequencing reveals heterogeneity of gastric cancer: progress and prospects. Front Oncol 2023;13:1074268.
[17] Wang X, Almet AA, Nie Q. The promising application of cell-cell interaction analysis in cancer from single-cell and spatial transcriptomics. Semin Cancer Biol 2023;95:42–51.
[18] Kumar V, Ramnarayanan K, Sundar R, et al. Single-cell atlas of lineage states, tumor microenvironment, and subtype-specific expression programs in gastric cancer. Cancer Discov 2022;12(3):670–91.
[19] Cristescu R, Lee J, Nebozhyn M, et al. Molecular analysis of gastric cancer identifies subtypes associated with distinct clinical outcomes. Nat Med 2015;21(5):449–56.
[20] Hao Y, Hao S, Andersen-Nissen E, et al. Integrated analysis of multimodal single-cell data. Cell 2021;184(13):3573–87. e3529.
[21] McGinnis CS, Murrow LM, Gartner ZJ. DoubletFinder: doublet detection in single-cell RNA sequencing data using artificial nearest neighbors. Cell Syst 2019;8(4):329–37. e324.
[22] Ianevski A, Giri AK, Aittokallio T. Fully-automated and ultra-fast cell-type identification using specific marker combinations from single-cell transcriptomic data. Nat Commun 2022;13(1):1246.
[23] Wang X, Zhou J, Li Z, et al. A novel pyroptosis-related prognostic signature for lung adenocarcinoma: Identification and multi-angle verification. Front Genet 2023;14:1160915.
[24] Yu G, Wang LG, Han Y, He QY. clusterProfiler: an R package for comparing biological themes among gene clusters. Omics: a J Integr Biol 2012;16(5):284–7.
[25] Newman AM, Steen CB, Liu CL, et al. Determining cell type abundance and expression from bulk tissues with digital cytometry. Nat Biotechnol 2019;37(7):773–82.
[26] Li J, Peng W, Yang P, et al. MicroRNA-1224-5p inhibits metastasis and epithelial-mesenchymal transition in colorectal cancer by targeting SP1-mediated NF-κB signaling pathways. Front Oncol 2020;10:294.
[27] Li J, Yang P, Chen F, et al. Hypoxic colorectal cancer-derived extracellular vesicles deliver microRNA-361-3p to facilitate cell proliferation by targeting TRAF3 via the noncanonical NF-κB pathways. Clin Transl Med 2021;11(3):e349.
[28] Bertheloot D, Latz E, Franklin BSNecroptosis. pyroptosis and apoptosis: an intricate game of cell death. Cell Mol Immunol 2021;18(5):1106–21.
[29] Chen R, Zeng L, Zhu S, et al. cAMP metabolism controls caspase-11 inflammasome activation and pyroptosis in sepsis. Sci Adv 2019;5(5):eaav5562.
[30] Rathinam VA, Fitzgerald KA. Inflammasome complexes: emerging mechanisms and effector functions. Cell 2016;165(4):792–800.
[31] van Deventer HW, Burgents JE, Wu QP, et al. The inflammasome component NLRP3 impairs antitumor vaccine by enhancing the accumulation of tumor-associated myeloid-derived suppressor cells. Cancer Res 2010;70(24):10161–9.
[32] Thrift AP, El-Serag HB. Burden of gastric cancer. Clin Gastroenterol Hepatol: Clin Pract J Am Gastroenterol Assoc 2020;18(3):534–42.
[33] Wong MCS, Huang J, Chan PSF, et al. Global incidence and mortality of gastric cancer, 1980-2018. JAMA Netw Open 2021;4(7):e2118457.
[34] Cao W, Chen HD, Yu YW, Li N, Chen WQ. Changing profiles of cancer burden worldwide and in China: a secondary analysis of the global cancer statistics 2020. Chin Med J 2021;134(7):783–91.
[35] Smyth EC, Nilsson M, Grabsch HI, van Grieken NC, Lordick F. Gastric cancer. Lancet (Lond, Engl) 2020;396(10251):635–48.
[36] Song H, Zhu J, Lu D. Molecular-targeted first-line therapy for advanced gastric cancer. Cochrane Database Syst Rev 2016;7(7). Cd011461.
[37] Patel TH, Cecchini M. Targeted therapies in advanced gastric cancer. Curr Treat Options Oncol 2020;21(9):70.
[38] Wang M, Zhao K, Liu M, et al. BMP4 preserves the developmental potential of mESCs through Ube2s- and Chmp4b-mediated chromosomal stability safeguarding. Protein Cell 2022;13(8):580–601.
[39] Bernareggi D, Xie Q, Prager BC, et al. CHMP2A regulates tumor sensitivity to natural killer cell-mediated cytotoxicity. Nat Commun 2022;13(1):1899.
[40] Takahashi Y, He H, Tang Z, et al. An autophagy assay reveals the ESCRT-III component CHMP2A as a regulator of phagophore closure. Nat Commun 2018;9(1):2855.
[41] Hattori T, Takahashi Y, Chen L, et al. Targeting the ESCRT-III component CHMP2A for noncanonical Caspase-8 activation on autophagosomal membranes. Cell Death Differ 2021;28(2):657–70.
[42] In H, Solsky I, Palis B, Langdon-Embry M, Ajani J, Sano T. Validation of the 8th Edition of the AJCC TNM staging system for gastric cancer using the national cancer database. Ann Surg Oncol 2017;24(12):3683–91.
[43] Mushti SL, Mulkey F, Sridhara R. Evaluation of overall response rate and progression-free survival as potential surrogate endpoints for overall survival in immunotherapy trials. Clin Cancer Res: J Am Assoc Cancer Res 2018;24(10):2268–75.
[44] Hu X, Wang J, Chu M, Liu Y, Wang ZW, Zhu X. Emerging role of ubiquitination in the regulation of PD-1/PD-L1 in cancer immunotherapy. Mol Ther: J Am Soc Gene Ther 2021;29(3):908–19.
[45] Li J, Sun J, Zeng Z, et al. Tumour-associated macrophages in gastric cancer: From function and mechanism to application. Clin Transl Med 2023;13(8):e1386.
[46] Sakaguchi S, Mikami N, Wing JB, Tanaka A, Ichiyama K, Ohkura N. Regulatory T cells and human disease. Annu Rev Immunol 2020;38:541–66.
[47] Xia L, Feng M, Ren Y, et al. DSE inhibits melanoma progression by regulating tumor immune cell infiltration and VCAN. Cell death Discov 2023;9(1):373.
[48] Yang L, Zhou YN, Zeng MM, et al. Circular RNA Circ-0002570 accelerates cancer progression by regulating VCAN via MiR-587 in gastric cancer. Front Oncol 2021;11:733745.